

1 Abundance compensates kinetics: 2 Similar effect of dopamine signals on 3 D1 and D2 receptor populations

4 Lars Hunger^{1*}, Arvind Kumar², Robert Schmidt¹

*For correspondence:
lhunger1@sheffield.ac.uk;
Lars.Hunger.314@gmail.com

5 ¹Department of Psychology, University of Sheffield; ²Department of
6 Computational Science and Technology, KTH Stockholm

8 **Abstract** The properties of different dopamine receptors constrain the function of
9 dopamine signals in the striatum of the basal ganglia. Still, dopamine receptor kinetics
10 are often neglected in considerations of the temporal dynamics of dopamine signalling.
11 Here we develop a neurochemical model of dopamine receptor binding taking into
12 account slow receptor kinetics. Contrary to current views, in our model D1 and D2
13 dopamine receptor populations react very similarly to dopamine signals independent of
14 their timescale and integrate them over minutes. Furthermore, our model explains why
15 ramping dopamine concentrations, observed experimentally, are an effective signal for
16 increasing the occupancy of dopamine receptors.

18 Introduction

19 The neuromodulator dopamine (DA) has complex effects on the activity of striatal neurons
20 by changing their excitability (*Day et al., 2008*) and strength of synaptic inputs (*Reynolds*
21 *et al., 2001*) in the context of motor control (*Syed et al., 2016*), action-selection (*Redgrave*
22 *et al., 2010*), reinforcement learning (*Schultz, 2007*), and addiction (*Everitt and Robbins,*
23 *2005*). Striatal DA concentration ([DA]) may change over multiple timescales (*Schultz,*
24 *2007*). Fast, abrupt increases in [DA] lasting for $\approx 1 - 3s$ result from phasic bursts in DA
25 neurons (*Roitman et al., 2004*), which signal reward-related information (*Schultz, 2007;*
26 *Grace et al., 2007*). Slightly slower [DA] ramps occur when rats approach a goal location
27 (*Howe et al., 2013*) or perform a reinforcement learning task (*Hamid et al., 2016*). Finally,
28 slow tonic spontaneous firing of DA neurons controls the baseline [DA] and may change
29 on a timescale of minutes or longer (*Grace et al., 2007*). However, whether fast and
30 slow changes in [DA] actually represent distinct signalling modes, e.g. for learning and
31 motivation (*Niv et al., 2007*), has recently been challenged (*Berke, 2018*). Furthermore, DA
32 acts on two different main receptor types, D1 and D2, adding another layer of complexity
33 to its signalling.

34 Based on different DA affinities of D1 and D2 receptors (D1R and D2R), it is often
35 assumed that striatal medium spiny neurons (MSN) respond differently to tonic and
36 phasic DA changes, depending on which DA receptor they express predominantly (*Dreyer*
37 *et al., 2010; Surmeier et al., 2007; Grace et al., 2007; Schultz, 2007; Frank and O'Reilly,*

2006). According to this "affinity-based" model the low affinity D1Rs (i.e. high dissociation
constant $K_D^{D1} = 1.6\mu M$; *Richfield et al., 1989*) cannot detect tonic changes in [DA] because
the fraction of occupied D1Rs is small ($\approx 1\%$) at baseline [DA] ($20nM$), see Methods) and
does not change much during tonic, low amplitude [DA] changes. However, D1Rs seem
well suited to detect phasic, high amplitude [DA] increases because they saturate at very
high [DA]. By contrast, D2Rs have a high affinity (i.e. low dissociation constant $K_D^{D2} = 25nM$;
Richfield et al., 1989) leading to $\approx 40\%$ of D2Rs being occupied at baseline [DA] ($20nM$).
Due to their high affinity, D2Rs can detect low amplitude, tonic increases/decreases in
[DA]. However, as D2Rs saturate at a relatively low $[DA] > 2 \cdot K_D^{D2}$, they seem unable to
detect high amplitude, phasic increases in [DA]. This suggests that D1 and D2 type MSNs
differentially encode phasic and tonic changes in [DA] solely because of the different
affinities of D1Rs and D2Rs (*Schultz, 2007*). However, this view is incompatible with recent
findings that D2R expressing MSNs can detect phasic changes in [DA] (*Yapo et al., 2017*;
Marcott et al., 2014).

The affinity-based model assumes that the reaction equilibrium is reached instantaneously,
whereby the receptor binding affinity can be used to approximate the fraction of receptors
bound to DA. However, this assumption holds only if the receptor kinetics are fast with
respect to the timescale of the DA signal, which is typically not the case. For instance,
D1Rs and D2Rs unbind from DA with a half-life time of $t_{1/2} \approx 80s$ (*Burt et al., 1976*;
Sano et al., 1979; *Maeno, 1982*; *Nishikori et al., 1980*), much longer than phasic signals
of a few seconds (*Robinson et al., 2001*; *Schultz, 2007*; *Hamid et al., 2016*). Moreover,
the fraction of bound receptors might be a misleading measure for the effect of DA signals,
since the abundances of D1R and D2R are quite different (see below). Therefore, we
developed a model of receptor binding based on the kinetics and abundances of D1Rs
and D2Rs to re-evaluate current views on DA signalling in the striatum.

Results and Discussion

To provide a realistic description of receptor kinetics, the binding and unbinding rates that
determine the receptor affinity are required. The available experimental measurements
indicate that the different D1R and D2R affinities are largely due to different binding rates,
while their unbinding rates are similar (*Burt et al., 1976*; *Sano et al., 1979*; *Maeno, 1982*;
Richfield et al., 1989). We incorporated these measurements into our slow kinetics model
(see Methods) and investigated the model in a variety of scenarios mimicking DA signals
on different timescales.

Firstly, to examine our model at baseline [DA], we investigated receptor binding
for a range of affinities (**Fig. 1a**), reflecting the range of measured values in different
experimental studies (*Neve and Neve, 1997*). We report the resulting receptor occupancy
in terms of the concentration of D1Rs and D2Rs bound to DA (denoted as $[D1 - DA]$
and $[D2 - DA]$, respectively). Due to the low affinity of D1Rs, slow changes in [DA] only
lead to small changes in the fraction of bound D1 receptors. However, there are overall
more D1Rs than D2Rs (*Richfield et al., 1989*), and $\approx 80\%$ of D2Rs are retained in the
endoplasmic reticulum (*Prou et al., 2001*). Therefore, the concentration of D1Rs in the
membrane available to extracellular DA is a lot higher than the concentration of D2Rs
(e.g. 20 times more in the nucleus accumbens; *Nishikori et al., 1980*; Methods). Thus,
in our simulation, the actual concentration of bound D1Rs ($[D1 - DA] \approx 20nM$) was, at
DA baseline, much closer to the concentration of bound D2Rs ($[D2 - DA] \approx 35nM$) than

83 suggested by the different D1 and D2 affinities alone. We further confirmed that this was
 84 not due to a specific choice of the dissociation constants in the model, as $[D1 - DA]$ and
 85 $[D2 - DA]$ remained similar over the range of experimentally measured D1R and D2R
 86 affinities (*Neve and Neve, 1997*) (**Fig. 1a**). This suggests that $[D1 - DA]$ is at most twice as
 87 high as $[D2 - DA]$ instead of 40 times higher as suggested by the difference in fraction
 88 of bound receptors. Therefore, $[D1 - DA]$ and $[D2 - DA]$ might be better indicators for
 89 the signal transmitted to MSNs as the fraction of bound receptors neglects the different
 90 receptor type abundances.

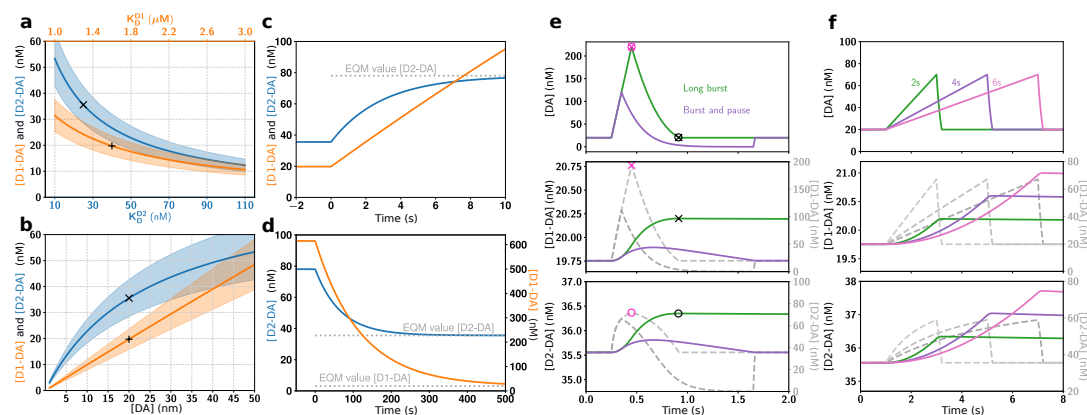


Figure 1. Impact of slow kinetics on D1R and D2R binding. **(a, b)** Equilibrium values of absolute concentration of receptors bound to DA vary as a function of receptor affinities (a) and baseline $[DA]$ (b), but are overall similar for D1 and D2 receptors. In (a) baseline $[DA]$ was fixed at 20 nM, and in (b) $K_D^{D1} = 1.6 \mu M$ and $K_D^{D2} = 25 nM$. 'x' and '+' indicate the model default parameters. Coloured bands mark the range of values for up to $\pm 20\%$ different receptor abundances. **(c)** For a large step up from $[DA] = 20 nM$ to $[DA] = 1 \mu M$, and **(d)** a step down from $[DA] = 1 \mu M$ to $[DA] = 20 nM$, D1 and D2 receptor occupancy approached their new equilibrium (EQM, grey dotted lines) only slowly (i.e. over seconds to minutes). **(e, f)** Effect of different phasic DA signals (top panels) is very different in the slow kinetics model (coloured traces in middle and bottom panels; left scales) compared to the instant kinetics model (dashed grey traces, right scales). The timing of the maximum receptor occupancy ('x' and 'o' for D1 and D2, respectively) coincides for instant kinetics (purple symbols) with the $[DA]$ peak (combined x and o in top panel), while for slow kinetics (black symbols) it coincides with the offset of the $[DA]$ signal instead (combined x and o in top panel).

91 Next, we investigated the effect of slow $[DA]$ changes (*Grace, 1995; Schultz, 1998;*
 92 *Floresco et al., 2003*) by exposing our model to changes in the $[DA]$ baseline. For signalling
 93 timescales that are long with respect to the half-life time of the receptors ($t_{slow} \gg t_{1/2} \approx$
 94 $80s$), we used the dissociation constant to calculate the steady state receptor occupancy.
 95 We found that for slow changes to a range of $[DA]$ baselines, $[D1 - DA]$ and $[D2 - DA]$ were
 96 also similar (**Fig. 1b**). Thus, we conclude that D1R and D2R occupancy reacts similarly
 97 to slow, low amplitude $[DA]$ changes because of the different abundances of D1 and D2
 98 receptors. This is contrary to instant kinetics models, suggesting that D2Rs are better
 99 suited to encode slow or tonic changes in $[DA]$.

100 To study the impact of faster $[DA]$ signals, we measured the step response of the
 101 model to a $[DA]$ change from 20nM to $1 \mu M$. This is quite a large change compared to
 102 phasic DA signals in vivo (*Robinson et al., 2001; Cheer et al., 2007; Hamid et al., 2016*),
 103 which we choose to illustrate that our results are not just due to a small amplitude DA
 104 signal. We found that binding to both receptor subtypes increased very slowly. Even for

105 the high affinity D2Rs it took more than 5s to reach their new equilibrium (**Fig. 1c**). Thus,
106 unlike the instant kinetics model, our model suggests that the D2Rs will not saturate for
107 single reward events, which last overall for up to $\approx 3s$. Note that the non-saturation is
108 independent of the abundance of the receptors and is only determined by the kinetics
109 of the receptors (see Methods). Due to their slow unbinding, D1Rs and D2Rs also took a
110 long time to return to baseline receptor occupancy after a step down from $[DA] = 1\mu M$
111 to $[DA] = 20nM$ (**Fig. 1d**). Thus, we conclude that with slow kinetics of receptor binding
112 both D1Rs and D2Rs can detect single phasic DA signals and that both remain occupied
113 long after the $[DA]$ has returned to baseline.

114 Next, we investigated $[D1 - DA]$ and $[D2 - DA]$ for a phasic DA increase (mimicking
115 reward responses; *Robinson et al., 2001; Cheer et al., 2007*), a phasic DA increase followed
116 by a decrease (mimicking responses to non-reward, salient stimuli; *Schultz, 2016*), and
117 a prolonged DA ramp (mimicking goal approach; *Howe et al., 2013; Hamid et al., 2016*).
118 In the instant kinetics model the D1Rs mirrored the $[DA]$ time course, since even at
119 $[DA] = 200nM$ they are far from saturation, whereas the D2Rs showed saturation effects
120 as soon as $[DA] > 2 \cdot K_D^{D2}$, leading to differing D1 and D2 time courses (**Fig. 1e, f**).
121 Importantly, in our model with slow kinetics, the time courses of $[D1 - DA]$ and $[D2 - DA]$
122 were similar for each of the three types of phasic DA signals.

123 While in our model we assumed slow kinetics based on neurochemical estimates
124 of wildtype DA receptors (*Burt et al., 1976; Sano et al., 1979; Maeno, 1982*), recent
125 genetically-modified DA receptors, used to probe $[DA]$ changes, have apparent fast ki-
126 netics (*Sun et al., 2018; Patriarchi et al., 2018*). Although their kinetics strongly changed
127 between receptor variants and may not reflect the kinetics of the wildtype receptor, we
128 examined our model also in the context of faster DA kinetics and found that the similarity
129 between $[D1 - DA]$ and $[D2 - DA]$ can be observed even if the actual kinetics were a 100
130 times faster than assumed in our model (**Supp. Fig. 1**). Therefore, our results do not
131 depend on the exact kinetics parameters or potential temperature effects, as long as the
132 parameter changes are roughly similar for D1 and D2 receptors. Furthermore, taking into
133 account different affinity states for D1Rs and D2Rs (*Richfield et al., 1989*), preserved the
134 similarity of time courses of D1R and D2R occupancy (**Supp. Fig. 7**). Finally, pauses in the
135 DA firing following aversive stimuli (*Schultz, 2007*) that lead to reductions in $[DA]$ (*Roitman*
136 *et al., 2008*), also have a similar effect on D1R and D2R occupancy (**Supp. Fig. 4e**).

137 Another striking effect of incorporating receptor kinetics was that a phasic increase
138 in $[DA]$ kept the receptors occupied for a long time (**Fig. 1e**). However, when a phasic
139 increase was followed by a decrease, $[D1 - DA]$ and $[D2 - DA]$ quickly returned to base-
140 line. This indicates that burst-pause firing patterns observed in DA cells for aversive or
141 salient non-rewarding signals (*Schultz, 2016*) can be distinguished from pure burst firing
142 patterns (which only lead to a phasic increase in $[DA]$) on the level of the MSN DA receptor
143 occupancy. This supports the view that the fast component of the DA firing patterns
144 (*Schultz, 2016*) is a salience response, and points to the intriguing possibility that the
145 pause following the burst can, at least partly, revoke the receptor-ligand binding induced
146 by the burst (see also **Supp. Fig. 2**). This effect even persists in a sequence of burst and
147 burst-pause events (**Supp. Fig. 5**). Thereby, the burst-pause firing pattern of DA neurons
148 could effectively signal a reward false-alarm.

149 The similarity of $[D1 - DA]$ and $[D2 - DA]$ responses to both slow and fast $[DA]$ changes
150 indicates that the different DA receptors respond similarly independent of the timescale

151 of [DA] changes. To understand why the D1Rs and D2Rs respond similarly, we considered
152 the relevant model parameters in more detail. The binding rate constants of D1Rs
153 and D2Rs differ by a factor of ≈ 60 ($k_{on}^{D1} = 0.0003125nm^{-1}min^{-1}$ and $k_{on}^{D2} = 0.02nm^{-1}min^{-1}$
154 ; *Burt et al., 1976*; *Sano et al., 1979*; *Maeno, 1982*; Methods), suggesting faster D2Rs.
155 However, experimental data suggests that there are ≈ 40 fold more unoccupied D1
156 receptors ($\approx 1600nM$) than unoccupied D2 receptors ($\approx 40nM$) on MSN membranes in
157 the extracellular space of the rat striatum (*Nishikori et al., 1980*). Therefore, the absolute
158 binding rate $\frac{d[DX-DA]^+}{dt} = k_{on} \cdot [DA] \cdot [DX]$ differs only by a factor of ≈ 1.5 between the
159 D1Rs and D2Rs. That is, the difference in the kinetics of D1Rs and D2Rs is compensated
160 by the different receptor numbers, resulting in nearly indistinguishable aggregate kinetics
161 (**Fig. 1e, f**). This is consistent with recent experimental findings that D2R expressing MSNs
162 can detect phasic [DA] signals (*Yapo et al., 2017*; *Marcott et al., 2014*).

163 Incorporating the slow kinetics in the model is crucial for functional considerations of
164 the DA system. Currently, following the instant kinetics model, the amplitude of a DA signal
165 (i.e. peak [DA]) is often considered as a key signal e.g. in the context of reward magnitude
166 or probability (*Hamid et al., 2016*; *Tobler et al., 2005*; *Morris et al., 2004*). However, as DA
167 unbinds slowly (over tens of seconds; **Fig. 1d**) and the binding rate changes approximately
168 linearly with [DA], the amount of receptor occupancy primarily depended on the area
169 under the curve of the [DA] signal (**Supp. Fig. 3**). Therefore, DA ramps, even with a
170 relatively small amplitude (**Fig. 1f** and **Supp. Fig. 4**), were very effective in increasing DA
171 receptor binding. In contrast, for locally very high [DA] (e.g. at corticostriatal synapses
172 during phasic DA cell activity; *Grace et al., 2007*) the high concentration gradient would
173 only lead to a very short duration of this local DA peak and thereby make it less effective
174 in occupying DA receptors.

175 The dynamics introduced by the slow kinetics had further effects on the timecourse of
176 DA signalling. With instant kinetics the maximum receptor occupancy was reached at the
177 peak [DA] (**Fig. 1e, f**). By contrast, for slow kinetics the maximum receptor occupancy was
178 reached when [DA] returned to its baseline (**Fig. 1e**) because as long as [DA] was higher
179 than the equilibrium value of [D1-DA] and [D2-DA], more receptors continued to become
180 occupied. Therefore for all DA signals, the maximum receptor occupancy was reached
181 towards the end of the pulse (**Fig. 1e, f** and **Supp. Fig. 4**).

182 Another effect of the slow kinetics was that DA receptors remained occupied long
183 after the DA pulse is over (**Fig. 1e, f**). This allowed the integration of DA pulses over
184 minutes (**Fig. 2a, b** and **Supp. Fig. 5**). We investigated potential functional consequences
185 of this integration by exposing the model to a sequence of trials modeling a simple
186 behavioural experiment with stochastic rewards (**see Methods**). We found that both D1R
187 and D2R occupancy coded for reward probability (**Fig. 2** and **Supp. Fig. 6**), consistent
188 with functional roles of DA signalling in motivation. However, this does not preclude
189 potential DA roles on shorter time scales, such as the invigoration of movements (*Roesch*
190 *et al., 2009*) or fast updates of state value (*Hamid et al., 2016*), as a sensitive readout
191 mechanism could also detect small increases in [D1-DA] and [D2-DA] (*Lamb and Pugh Jr,*
192 *1992*).

193 Overall, our slow kinetics model of DA receptor binding casts doubt on several long-
194 held views on DA signalling. Our model indicates that both D1R and D2R systems can
195 detect [DA] changes, independent of the timescale, equally well. Although, D1Rs and
196 D2Rs have opposing effects on the excitability (*Flores-Barrera et al., 2011*) and strength

197 of cortico-striatal synapse of D1 and D2 type MSNs (*Centonze et al., 2001*), we challenge
198 the current view that differences in receptor affinity introduce additional asymmetries in
199 D1 and D2 signalling. Instead of listening to different components of the DA signal, D1
200 and D2 MSNs seem to respond to the same DA input, increasing the differential effect on
201 firing rate response of D1 and D2 MSNs.
202

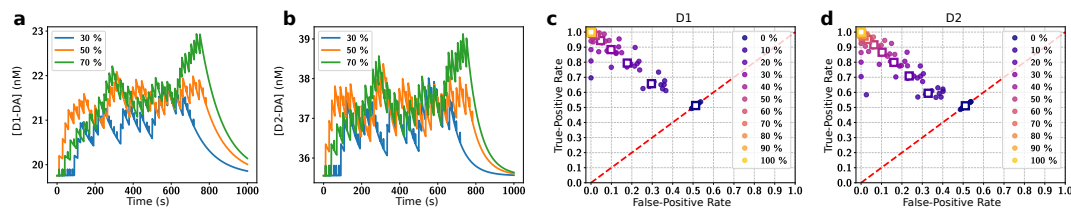


Figure 2. Integration of DA signals over minutes in a simulation of a behavioural task. **(a, b)** Timecourse of D1 (a) and D2 (b) receptor occupancy for sequences of 50 trials with a reward probability, as indicated, in each trial. Rewarded trials were modelled with a long DA burst, non-rewarded trials with a burst-pause DA timecourse. **(c, d)** Decoding accuracy of the difference in reward probability based on the D1 (c) and D2 (d) receptor occupancy by a simple classifier. Each data point indicates the decoding accuracy from a simulation scenario with the difference in reward probability indicated by the colour. Single dots correspond to simulations with different absolute reward probabilities. The colour indicates the difference in reward probability (e.g. a 10% difference in purple occurs for 80% vs. 90%, 70% vs. 80%, etc.), and the squares denote the corresponding averages. Red line indicates chance level performance, and a perfect classifier would be at 1.0 true and 0.0 false positive rate. Note that the classification is similar for D1 and D2 receptors, yielding near perfect classification already at 40% reward difference.

203 Methods and Materials

204 The models were implemented in Python. The scripts used to generate the data and
205 figures can be accessed here: https://bitbucket.org/Narur/abundance_kinetics/src/.

206 Kinetics model

207 In the instant kinetics model the fraction of occupied D1 and D2 receptors (f_{D1} and f_{D2})
208 are calculated directly from the concentration of free DA in the extracellular space, $[DA]$,
209 and the dissociation constant K_D :

$$f = \frac{[DA]}{K_D + [DA]}. \quad (1)$$

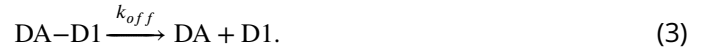
210 However, the dissociation constant is an equilibrium constant, so it should only be used
211 for calculating the receptor occupancy when the duration of the DA signal is longer than
212 the time needed to reach the equilibrium. As this is typically not the case for phasic DA
213 signals (see main text), we developed a model incorporating slow kinetics.

When DA and one of its receptors are both present in a solution they constantly bind and unbind. During the binding a receptor ligand complex (here called DA–D1 or DA–D2) is formed. We call the receptor ligand complex an occupied DA receptor. Note that although in the following part we provide the equations for D1 receptors, the same equations apply for D2 receptors (with different kinetic parameters). In a solution binding

occurs when receptor and ligand meet due to diffusion, with high enough energy and a suitable orientation, described as:



Accordingly, unbinding of the complex is denoted as:



The kinetics of this binding and unbinding, treated here as first-order reactions, are governed by the rate constants k_{on} and k_{off} that are specific for a receptor ligand pair and temperature dependent. Since both processes are happening simultaneously we can write this as:



The rate at which the receptor is occupied depends on $[DA]$, the concentration of free receptor $[D1]$ and the binding rate constant k_{on} :

$$\frac{d[DA - D1]^+}{dt} = k_{on} \cdot [DA] \cdot [D1]. \quad (5)$$

The rate at which the receptor-ligand complex unbinds is given by concentration of the complex $[DA - D1]$ and the unbinding rate constant k_{off} :

$$\frac{d[DA - D1]^-}{dt} = -k_{off} \cdot [DA - D1]. \quad (6)$$

The equilibrium is reached when the binding and unbinding rates are equal, so by combining Eq. 5 and Eq. 6 we obtain:

$$k_{on} \cdot [DA] \cdot [D1] = k_{off} \cdot [DA - D1]. \quad (7)$$

At the equilibrium the dissociation constant K_D is defined as:

$$K_D = \frac{[DA] \cdot [D1]}{[DA - D1]} = \frac{k_{off}}{k_{on}}. \quad (8)$$

214 When half of the receptors are occupied, i.e. $[DA - D1] = [D1]$, Eq. 8 simplifies to $K_D = [DA]$.
 215 So at equilibrium, K_D is the ligand concentration at which half of the receptors are
 216 occupied.

217 Importantly, for fast changes in $[DA]$ (i.e. over seconds) it takes some time until the
 218 changed binding (Eq. 5) and unbinding rates (Eq. 6) are balanced, so the new equilibrium
 219 will not be reached instantly. The timescale in which equilibrium is reached can be
 220 estimated from the half-life time of the bound receptor. The half-life time assumes an
 221 exponential decay process as described in Eq. 6 and is the time required so that half of
 222 the currently bound receptors unbind. If $[DA] = 0$, and there is no more binding, the half
 223 life time of the receptors can be calculated from the off-rate by using $t_{1/2} = \ln(2)/k_{off}$.
 224 Signal durations should be of the same order of magnitude (or longer) than the half-life
 225 time in order for the instant kinetics model to be applicable.

We calculated the time course of occupied receptor after an abrupt change in $[DA]$ by integrating the rate equation, given by the sum of Eq. 5 and Eq. 6:

$$\frac{d[DA - D1]}{dt} = k_{on}[DA][D1] - k_{off}[DA - D1]. \quad (9)$$

To integrate Eq. 9 we substitute

$$[D1] = [D1^{tot}] - [DA - D1] \quad (10)$$

226 where $[D1^{tot}]$ is the total amount of D1 receptor (bound and unbound to DA) on the cell
 227 membranes available for binding to extracellular DA.

228 To model the effect of phasic changes in $[DA]$ we choose the initial receptor occupancy
 229 $[DA - D1](t = 0) = [DA - D1]^0$ and the receptor occupancy for the new equilibrium at time
 230 infinity $[DA - D1](t = \infty) = [DA - D1]^\infty$ as the boundary conditions. With these boundary
 231 conditions we get an expression for the time evolution of the receptor occupancy under
 232 the assumption that binding to the receptor does not significantly change the free $[DA]$:

$$\begin{aligned} [DA - D1](t) = & \\ & ([DA - D1]^0 - [DA - D1]^\infty) \cdot e^{-(k_{on}[DA] + k_{off})t} \\ & + [DA - D1]^\infty. \end{aligned} \quad (11)$$

233 For our slow kinetics model we solved Eq. 9 for each receptor type and arbitrary DA
 234 timecourses numerically employing a 4th order Runge Kutta solver with a 1 ms time
 235 resolution.

236 We did not take into account the change in $[DA]$ caused by the binding and unbinding
 237 to the receptors since the rates at which DA is removed from the system by binding to the
 238 receptors is much slower than the rate of DA being removed from the system by uptake
 239 through DA transporters. For example the rate at which DA binds to the receptors is:

$$\begin{aligned} \frac{([DA - D1] + [DA - D2])}{dt} = & \\ & k_{on}^{D1}[DA][D1] + k_{on}^{D2}[DA][D2] \\ & = -\frac{[DA]}{dt}. \end{aligned} \quad (12)$$

At a DA concentration of $[DA] = 1\mu M$ with a D1 and D2 occupancy of $[DA - D1] \approx 20.0nM$ and $[DA - D2] \approx 40nM$ (the equilibrium values for $[DA] = 20nM$) and $k_{on}^{D1} = 5.2 \cdot 10^{-6}nM^{-1}s^{-1}$, $k_{on}^{D2} = 3.3 \cdot 10^{-4}nM^{-1}s^{-1}$, $[D1] \approx 1600.0nM$, $[D2] \approx 40.0nM$ and $[DA] = 1\mu M$ the rate of DA removal through binding to the receptors is:

$$\frac{[DA]^{binding}}{dt} = -23.6nM/s. \quad (13)$$

However, the DA removal rate by Michaelis-Menten uptake through the DA transporters at this concentration would be:

$$\frac{[DA]^{uptake}}{dt} = V_{max} \frac{[DA]}{[DA] + K_m} \quad (14)$$

$$= -4.0 \frac{\mu M}{s} \cdot \frac{1\mu M}{1\mu M + 0.21\mu M} \quad (15)$$

$$= -3.3 \frac{\mu M}{s}. \quad (16)$$

240 Where V_{max} is the maximal uptake rate, and K_m the Michaelis-Menten constant describing
 241 the $[DA]$ concentration at which uptake is at half the maximum rate. As $\left| \frac{[DA]^{uptake}}{dt} \right| \gg$

242 $\left| \frac{[DA]^{binding}}{dt} \right|$, the DA dynamics are dominated by the uptake process and not by binding to
243 the receptors. Therefore, we neglected the receptor-ligand binding for the DA dynamics
244 in our model. However, for faster DA receptors this effect would become more important.

245 Receptor parameters

An important model parameter is the total concentration of the D1 and D2 receptors on the membrane ($[D1]^{tot}$ and $[D2]^{tot}$) that can bind to DA in the extracellular space of the striatum. Our estimate of $[D1]^{tot}$ and $[D2]^{tot}$ is based on radioligand binding studies in the rostral striatum (*Richfield et al., 1989, 1987*). We use the following equation, in which X is a placeholder for the respective receptor type, to calculate these concentrations.

$$[DX]^{tot} = [DX]^m \cdot \frac{\epsilon \cdot f_{DX}^{membrane}}{\alpha \rho_{brain}} \quad (17)$$

246 The experimental measurements provide us with a the number of receptors per
247 unit of protein weight $[D1]^m$ and $[D2]^m$. To transform these measurements into molar
248 concentrations for our simulations, we multiply by the protein content of the wet weight
249 of the rat caudate nucleus ϵ , which is around 12% (*Banay-Schwartz et al., 1992*). This
250 leaves us with the amount of protein per g of wet weight of the rat brain. Next we
251 divide by the average density of a rat brain which is $\rho_{brain} = 1.05g/ml$ (*DiResta et al.,*
252 *1990*) to find the amount of receptors per unit of volume of the rat striatum. Finally, we
253 divide by the volume fraction α , the fraction of the brain volume that is taken up by the
254 extracellular space in the rat brain, to obtain the receptor concentration of the receptor
255 in the extracellular medium. The procedure ends here for the D1 receptors since there
256 is no evidence that D1 receptors are internalized in the baseline state (*Prou et al., 2001*).
257 However, a large fraction of the D2 receptors is retained in the endoplasmatic reticulum
258 of the neuron (*Prou et al., 2001*), reducing the amount of receptors that contribute to
259 the concentration of receptors in the extracellular medium by $f^{membrane}$, the fraction of
260 receptors protruding into the extracellular medium.

261 In addition to the receptor concentration, the kinetic constants of the receptors are
262 key parameters in our slow kinetics model. In an equilibrium measurement in the canine
263 caudate nucleus the dissociation constant of low affinity DA binding sites, corresponding
264 to D1 receptors (*Maeno, 1982*), has been measured as $K_d = 1.6\mu M$ (*Sano et al., 1979*).
265 However, when calculating K_d (using Eq. 8) from the measured kinetic constants (*Sano*
266 *et al., 1979*) the value is $K_d^{D1} = 2.6\mu M$. To be more easily comparable to other simulation
267 works (*Dreyer et al., 2010*) and direct measurements (*Richfield et al., 1989; Sano et al.,*
268 *1979*) we choose $K_d^{D1} = 1.6\mu M$ in our simulations. For this purpose we modified both the
269 $k_{on}^{D1} = 0.00025min^{-1}nM^{-1}$ and $k_{off}^{D1} = 0.64min^{-1}$ rate measured (*Sano et al., 1979*) by $\approx 25\%$,
270 making $k_{on}^{D1} = 0.0003125min^{-1}nM^{-1}$ slightly faster and $k_{off}^{D1} = 0.5min^{-1}$ slightly slower, so
271 that the resulting $K_d^{D1} = 1.6\mu M$. The kinetic constants have been measured at 30 C and
272 are temperature dependent. In biological reactions a temperature change of 10 C is
273 usually associated with a change in reaction rate around a factor of 2-3 (*Reyes et al.,*
274 *2008*). However, the conclusions of this paper do not change for an increase in reaction
275 rates by a factor of 2 – 3 (see **Supp. Fig. 1**). It should also be noted that the measurement
276 of the commonly referenced K_d (*Richfield et al., 1989*) have been performed at room
277 temperature.

278 The kinetic constants for the D2 receptors were obtained from measurements at 37°C

279 of high affinity DA binding sites (*Burt et al., 1976*), which correspond to the D2 receptor
 280 (*Maeno, 1982*). The values are $k_{on}^{D2} = 0.02 \text{min}^{-1} \text{nM}^{-1}$ and $k_{off}^{D2} = 0.5 \text{min}^{-1}$, which yields
 281 $K_D^{D2} = 25 \text{nM}$, in line with the values measured in (*Richfield et al., 1989*). As the off-rate of
 282 the D1 and D2 receptors $k_{off}^{D1} = 0.64 \text{min}^{-1} \text{nM}^{-1}$ and $k_{off}^{D2} = 0.5 \text{min}^{-1}$ is quite similar, the
 283 difference in $K_D^{D2} = 25 \text{nM}$ and $K_d^{D1} = 1.5 \mu\text{M}$ is largely due to differences in the on-rate
 284 of the receptors. This is important because the absolute rate of receptor occupancy
 285 depends linearly not only on the on-rate, but also on the receptor concentration (see
 286 Eq. 5), which means that a slower on-rate could be compensated for by a higher number
 287 of receptors.

Measured values		
Parameter		Source
$[D1]^m$ in pmol/mg protein	2840	(<i>Richfield et al., 1989</i>)
$[D2]^m$ in pmol/mg protein	696	(<i>Richfield et al., 1989</i>)
ϵ	0.12	(<i>Banay-Schwartz et al., 1992</i>)
α	0.2	(<i>Syková and Nicholson, 2008</i>)
ρ_{brain} in g/ml	1.05	(<i>DiResta et al., 1990</i>)
$f_{D1}^{membrane}$	1.0	(<i>Prou et al., 2001</i>)
$f_{D2}^{membrane}$	0.2	(<i>Prou et al., 2001</i>)
$k_{on}^{D1,orig}$ in $\text{nm}^{-1} \text{min}^{-1}$	0.00025	(<i>Sano et al., 1979</i>)
$k_{off}^{D1,orig}$ in min^{-1}	0.64	(<i>Sano et al., 1979</i>)
k_{on}^{D2} in $\text{nm}^{-1} \text{min}^{-1}$	0.02	(<i>Burt et al., 1976</i>)
k_{off}^{D2} in min^{-1}	0.5	(<i>Burt et al., 1976</i>)
Derived Parameters		
Parameter		Source
$[D1]$ in nM	≈ 1600	Eq.(17)
$[D2]$ in nM	≈ 80	Eq.(17)
$k_{on}^{D1,used}$ in $\text{nm}^{-1} \text{min}^{-1}$	0.0003125	see Text
$k_{off}^{D1,used}$ in min^{-1}	0.5	see Text

Table 1. Receptor parameters

288 The parameters that we used in the simulations are summarized in Tab. 1.

289 Dopamine signals

290 In our model we assumed a baseline $[DA]$ of $[DA]^{tonic} = 20 \text{nM}$ (*Dreyer et al., 2010; Dreyer,*
 291 *2014; Venton et al., 2003; Saud-Chagny et al., 1992; Borland et al., 2005; Justice Jr, 1993;*
 292 *Atcherley et al., 2015*). We modelled changes in $[DA]$ to mimic DA signals observed in
 293 experimental studies. We use three types of single pulse DA signals: (long-)burst, burst-
 294 pause and ramp.

295 The burst signal mimics the result of a phasic burst in the activity of DA neurons in
 296 the SNc, e.g. in response to reward-predicting cues (*Pan et al., 2005*). The model burst
 297 signal consists of a rapid linear $[DA]$ increase (with an amplitude $\Delta[DA]$ and rise time t_{rise})
 298 and a subsequent return to baseline. The return to baseline is governed by Michaelis
 299 Menten kinetics with appropriate parameters for the dorsal striatum $V_{max} = 4.0 \mu\text{M s}^{-1}$ and
 300 $K_m = 0.21 \mu\text{M}$ (*Bergstrom and Garris, 2003*) and the nucleus accumbens $V_{max} = 1.5 \mu\text{M s}^{-1}$

301 (*Dreyer and Hounsgaard, 2013*). In our model the removal of DA is assumed to happen
302 without further DA influx into the system (baseline firing resumes when [DA] has returned
303 to its baseline value). Unless stated otherwise, the long-burst signals are used with a
304 $\Delta[DA] = 200 \text{ nM}$ and a rise time of $t_{rise} = 0.2 \text{ s}$ at $V_{max} = 1.5 \mu\text{M s}^{-1}$, similar to biologically
305 realistic transient signals (*Cheer et al., 2007; Robinson et al., 2001; Day et al., 2007*).

306 The burst-pause signal has two components, an initial short, small amplitude burst
307 ($\Delta[DA] = 100 \text{ nM}$, $t_{rise} = 0.1 \text{ s}$), with the corresponding [DA] return to baseline (as for the
308 long burst above). However, there is a second component in the DA signal, in which [DA]
309 falls below baseline, simulating a pause in DA neuron firing. The length of this firing pause
310 is characterized by the parameter t_{pause} . This burst-pause [DA] signal reflects the DA cell
311 firing pattern consisting of a brief burst followed by a pause in activity (*Pan et al., 2008;*
312 *Schultz, 2016*).

313 The ramp DA signal is characterized by the same parameters as the burst pattern, but
314 with a longer t_{rise} and a smaller $\Delta[DA]$.

315 **Behavioural task simulation**

316 To determine whether DA receptor occupancy can integrate reward signals over minutes,
317 we simulated sequences consisting of 50 trials. Each sequence had a fixed reward
318 probability. The trials contained either a long burst DA signal (mimicking a reward) or a
319 burst-pause DA signal (mimicking no reward) at the beginning of the trial according to the
320 reward probability of the sequence. The inter trial interval was $15 \pm 5 \text{ s}$ (**Fig. 2** and **Supp.**
321 **Fig. 6**). We choose this highly simplistic scenario to reflect DA signals in a behavioural task
322 in which the animal is rewarded for correct performance. However, here the specifics
323 of the task are not relevant as our model addresses the integration of the DA receptor
324 occupancy over time. Although we chose to use the burst-pause type signal as shown
325 in **Fig. 1e** as a non-rewarding event, the difference to a non-signal are minimal after the
326 end of the pause (**Supp. Figs. 2 and 5**). Each sequence started from a baseline receptor
327 occupancy, assuming a break between sequences long enough for the receptors to return
328 to baseline occupancy (around 5 minutes). For the simulations shown in **Supp. Fig. 5** all
329 trials started exactly 15 s apart.

330 We simulated all reward probabilities from 0% to 100% in 10% steps. For each reward
331 probability we ran 500 sequences, and calculated the mean receptor occupancy over time
332 (single realisations shown in **Fig. 2a, b**). To investigate whether the receptor occupancy
333 distinguished between different reward probabilities we applied a simple classifier to the
334 receptor occupancy timeline.

335 The classifier was used to compare two different reward probabilities at a time. At each
336 time point it was applied to a pair of receptor occupancies, e.g. one belonging to a 50% and
337 one to a 30% reward probability sequence. The classifier assigned the current receptor
338 occupancy to the higher or lower reward probability depending on which one was closer
339 to the mean (over 500 sequences) receptor occupancy of that reward probability. As we
340 knew the underlying reward probability of each sequence we were able to calculate the
341 true and false positive rates and accuracy for each time point in our set of 500 sequences
342 for both the D1R and D2R (**Supp. Fig. 6**). The accuracy was calculated based on all time
343 points between 200 and 800s within a sequence to avoid the effect of the initial “swing-in”
344 and post-sequence DA levels returning to baseline.

Acknowledgments

We thank Joshua Berke, Paul Overton, Alejandro Jimenez, Mohammadreza Mohagheghi Nejad and Amin Mirzaei for helpful discussions. This work was supported by the University of Sheffield and its high performance computing resources, the BrainLinks-BrainTools Cluster of Excellence funded by the German Research Foundation (DFG, grant number EXC 1086), and the state of Baden-Wuerttemberg through bwHPC.

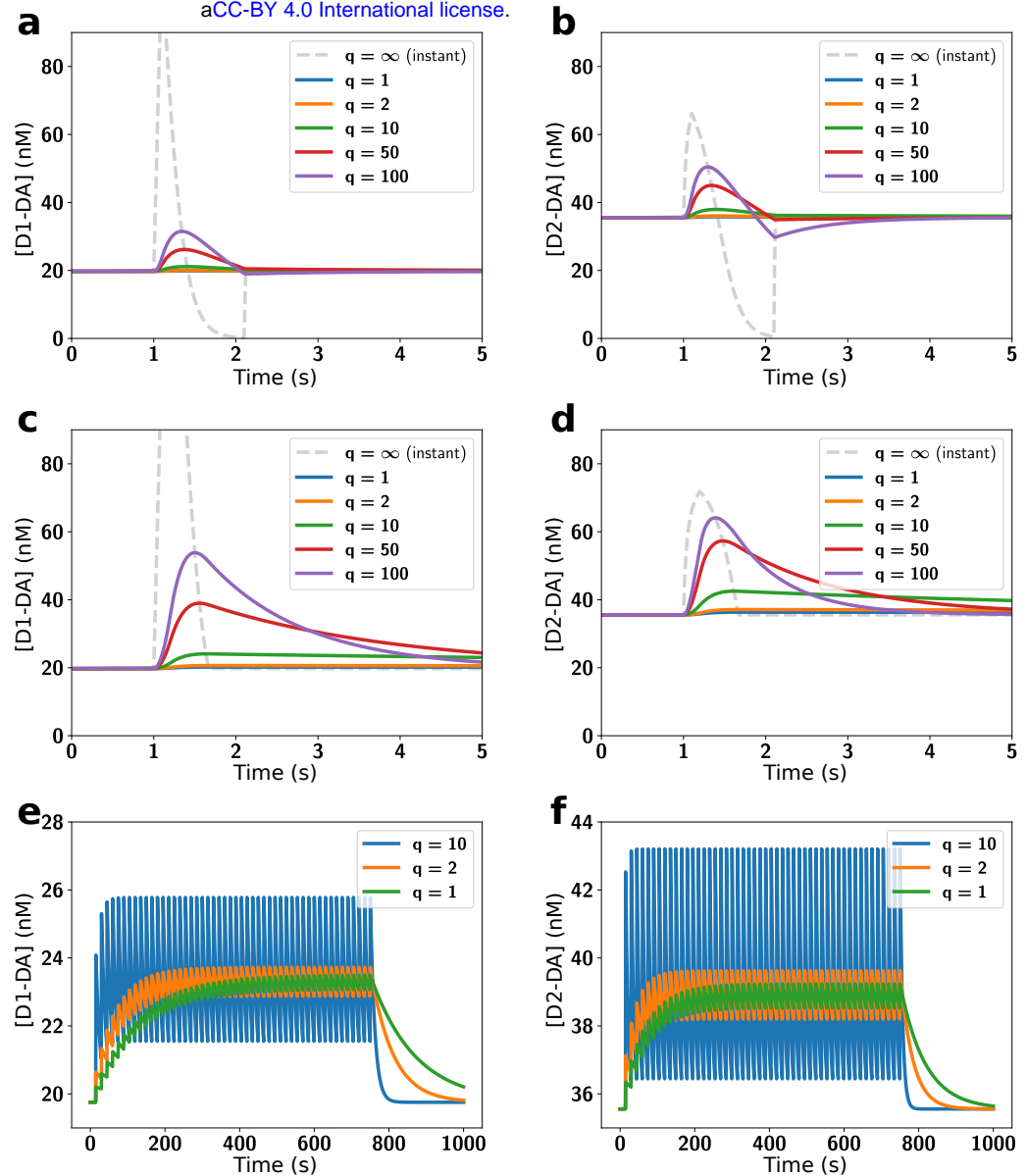
References

- Atcherley CW**, Wood KM, Parent KL, Hashemi P, Heien ML. The coaction of tonic and phasic dopamine dynamics. *Chemical Communications*. 2015; 51(12):2235–2238.
- Banay-Schwartz M**, Kenessey A, DeGuzman T, Lajtha A, Palkovits M. Protein content of various regions of rat brain and adult and aging human brain. *Age*. 1992; 15(2):51–54.
- Bergstrom BP**, Garris PA. 'Passive stabilization' of striatal extracellular dopamine across the lesion spectrum encompassing the presymptomatic phase of Parkinson's disease: a voltammetric study in the 6-OHDA-lesioned rat. *Journal of neurochemistry*. 2003; 87(5):1224–1236.
- Berke JD**. What does dopamine mean? *Nature neuroscience*. 2018; p. 1.
- Borland LM**, Shi G, Yang H, Michael AC. Voltammetric study of extracellular dopamine near microdialysis probes acutely implanted in the striatum of the anesthetized rat. *Journal of neuroscience methods*. 2005; 146(2):149–158.
- Burt DR**, Creese I, Snyder SH. Properties of [3H] haloperidol and [3H] dopamine binding associated with dopamine receptors in calf brain membranes. *Molecular pharmacology*. 1976; 12(5):800–812.
- Centonze D**, Picconi B, Gubellini P, Bernardi G, Calabresi P. Dopaminergic control of synaptic plasticity in the dorsal striatum. *European journal of neuroscience*. 2001; 13(6):1071–1077.
- Cheer JF**, Aragona BJ, Heien ML, Seipel AT, Carelli RM, Wightman RM. Coordinated accumbal dopamine release and neural activity drive goal-directed behavior. *Neuron*. 2007; 54(2):237–244.
- Day JJ**, Roitman MF, Wightman RM, Carelli RM. Associative learning mediates dynamic shifts in dopamine signaling in the nucleus accumbens. *Nature neuroscience*. 2007; 10(8):1020.
- Day M**, Wokosin D, Plotkin JL, Tian X, Surmeier DJ. Differential excitability and modulation of striatal medium spiny neuron dendrites. *Journal of Neuroscience*. 2008; 28(45):11603–11614.
- DiResta G**, Lee J, Lau N, Ali F, Galicich J, Arbit E. Measurement of brain tissue density using pycnometry. In: *Brain Edema VIII* Springer; 1990.p. 34–36.
- Dreyer JK**. Three mechanisms by which striatal denervation causes breakdown of dopamine signaling. *Journal of Neuroscience*. 2014; 34(37):12444–12456.
- Dreyer JK**, Herrik KF, Berg RW, Hounsgaard JD. Influence of phasic and tonic dopamine release on receptor activation. *Journal of Neuroscience*. 2010; 30(42):14273–14283.
- Dreyer JK**, Hounsgaard J. Mathematical model of dopamine autoreceptors and uptake inhibitors and their influence on tonic and phasic dopamine signaling. *Journal of neurophysiology*. 2013; 109(1):171–182.
- Everitt BJ**, Robbins TW. Neural systems of reinforcement for drug addiction: from actions to habits to compulsion. *Nature neuroscience*. 2005; 8(11):1481.

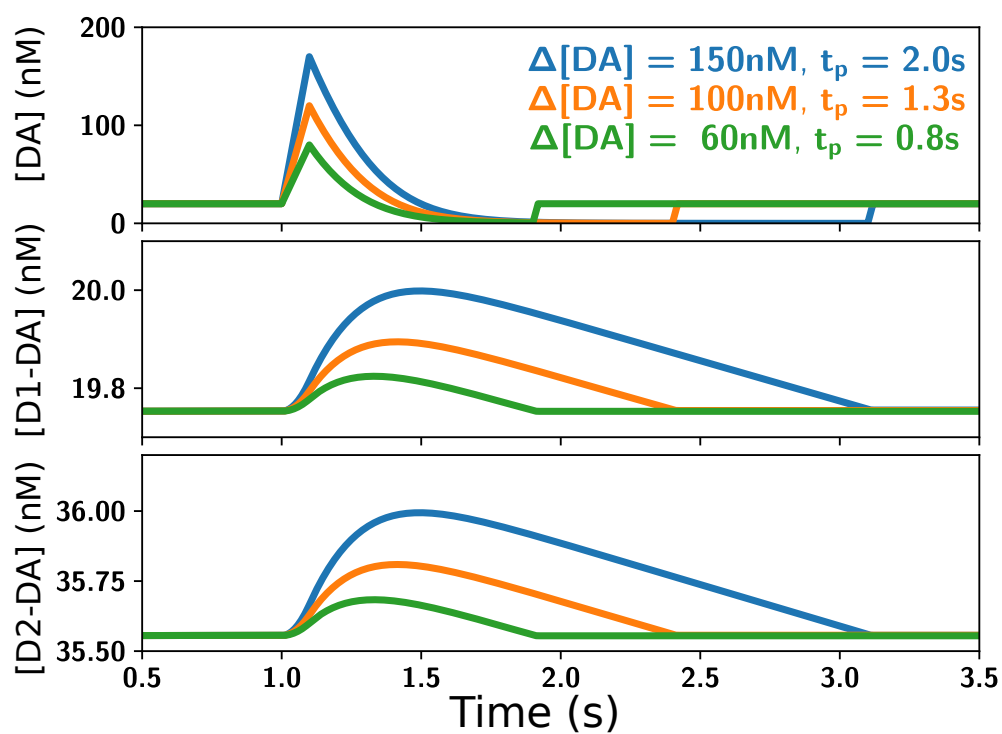
- 384 **Flores-Barrera E**, Vizcarra-Chacón BJ, Bargas J, Tapia D, Galarraga E. Dopaminergic modulation of
385 corticostriatal responses in medium spiny projection neurons from direct and indirect pathways.
386 *Frontiers in systems neuroscience*. 2011; 5:15.
- 387 **Floresco SB**, West AR, Ash B, Moore H, Grace AA. Afferent modulation of dopamine neuron firing
388 differentially regulates tonic and phasic dopamine transmission. *Nature neuroscience*. 2003;
389 6(9):968.
- 390 **Frank MJ**, O'Reilly RC. A mechanistic account of striatal dopamine function in human cognition:
391 psychopharmacological studies with cabergoline and haloperidol. *Behavioral neuroscience*. 2006;
392 120(3):497.
- 393 **Grace AA**. The tonic/phasic model of dopamine system regulation: its relevance for understanding
394 how stimulant abuse can alter basal ganglia function. *Drug & Alcohol Dependence*. 1995;
395 37(2):111–129.
- 396 **Grace AA**, Floresco SB, Goto Y, Lodge DJ. Regulation of firing of dopaminergic neurons and control
397 of goal-directed behaviors. *Trends in neurosciences*. 2007; 30(5):220–227.
- 398 **Hamid AA**, Pettibone JR, Mabrouk OS, Hetrick VL, Schmidt R, Vander Weele CM, Kennedy RT,
399 Aragona BJ, Berke JD. Mesolimbic dopamine signals the value of work. *Nature neuroscience*.
400 2016; 19(1):117.
- 401 **Howe MW**, Tierney PL, Sandberg SG, Phillips PE, Graybiel AM. Prolonged dopamine signalling in
402 striatum signals proximity and value of distant rewards. *Nature*. 2013; 500(7464):575–579.
- 403 **Justice Jr J**. Quantitative microdialysis of neurotransmitters. *Journal of neuroscience methods*.
404 1993; 48(3):263–276.
- 405 **Lamb T**, Pugh Jr E. G-protein cascades: gain and kinetics. *Trends in neurosciences*. 1992; 15(8):291–
406 298.
- 407 **Maeno H**. Dopamine receptors in canine caudate nucleus. *Molecular and cellular biochemistry*.
408 1982; 43(2):65–80.
- 409 **Marcott PF**, Mamaligas AA, Ford CP. Phasic dopamine release drives rapid activation of striatal
410 D2-receptors. *Neuron*. 2014; 84(1):164–176.
- 411 **Morris G**, Arkadir D, Nevet A, Vaadia E, Bergman H. Coincident but distinct messages of midbrain
412 dopamine and striatal tonically active neurons. *Neuron*. 2004; 43(1):133–143.
- 413 **Neve KA**, Neve RL. Molecular biology of dopamine receptors. In: *The dopamine receptors* Springer;
414 1997.p. 27–76.
- 415 **Nishikori K**, Noshiro O, Sano K, Maeno H. Characterization, solubilization, and separation of two
416 distinct dopamine receptors in canine caudate nucleus. *Journal of Biological Chemistry*. 1980;
417 255(22):10909–10915.
- 418 **Niv Y**, Daw ND, Joel D, Dayan P. Tonic dopamine: opportunity costs and the control of response
419 vigor. *Psychopharmacology*. 2007; 191(3):507–520.
- 420 **Pan WX**, Schmidt R, Wickens JR, Hyland BI. Dopamine cells respond to predicted events during
421 classical conditioning: evidence for eligibility traces in the reward-learning network. *Journal of*
422 *Neuroscience*. 2005; 25(26):6235–6242.
- 423 **Pan WX**, Schmidt R, Wickens JR, Hyland BI. Tripartite mechanism of extinction suggested by
424 dopamine neuron activity and temporal difference model. *Journal of Neuroscience*. 2008;
425 28(39):9619–9631.

- 426 **Patriarchi T**, Cho JR, Merten K, Howe MW, Marley A, Xiong WH, Folk RW, Broussard GJ, Liang R, Jang
427 MJ, et al. Ultrafast neuronal imaging of dopamine dynamics with designed genetically encoded
428 sensors. *Science*. 2018; p. eaat4422.
- 429 **Prou D**, Gu WJ, Le Crom S, Vincent JD, Salamero J, Vernier P. Intracellular retention of the two
430 isoforms of the D 2 dopamine receptor promotes endoplasmic reticulum disruption. *Journal of*
431 *Cell Science*. 2001; 114(19):3517–3527.
- 432 **Redgrave P**, Rodriguez M, Smith Y, Rodriguez-Oroz MC, Lehericy S, Bergman H, Agid Y, DeLong MR,
433 Obeso JA. Goal-directed and habitual control in the basal ganglia: implications for Parkinson's
434 disease. *Nature Reviews Neuroscience*. 2010; 11(11):760–772.
- 435 **Reyes BA**, Pendergast JS, Yamazaki S. Mammalian peripheral circadian oscillators are temperature
436 compensated. *Journal of biological rhythms*. 2008; 23(1):95–98.
- 437 **Reynolds JN**, Hyland BI, Wickens JR. A cellular mechanism of reward-related learning. *Nature*. 2001;
438 413(6851):67.
- 439 **Richfield EK**, Penney JB, Young AB. Anatomical and affinity state comparisons between dopamine
440 D 1 and D 2 receptors in the rat central nervous system. *Neuroscience*. 1989; 30(3):767–777.
- 441 **Richfield EK**, Young AB, Penney JB. Comparative distribution of dopamine D-1 and D-2 receptors in
442 the basal ganglia of turtles, pigeons, rats, cats, and monkeys. *Journal of Comparative Neurology*.
443 1987; 262(3):446–463.
- 444 **Robinson DL**, Phillips PE, Budygin EA, Trafton BJ, Garris PA, Wightman RM. Sub-second changes in
445 accumbal dopamine during sexual behavior in male rats. *Neuroreport*. 2001; 12(11):2549–2552.
- 446 **Roesch MR**, Singh T, Brown PL, Mullins SE, Schoenbaum G. Ventral striatal neurons encode the
447 value of the chosen action in rats deciding between differently delayed or sized rewards. *Journal*
448 *of Neuroscience*. 2009; 29(42):13365–13376.
- 449 **Roitman MF**, Stuber GD, Phillips PE, Wightman RM, Carelli RM. Dopamine operates as a subsecond
450 modulator of food seeking. *Journal of Neuroscience*. 2004; 24(6):1265–1271.
- 451 **Roitman MF**, Wheeler RA, Wightman RM, Carelli RM. Real-time chemical responses in the nucleus
452 accumbens differentiate rewarding and aversive stimuli. *Nature neuroscience*. 2008; 11(12):1376.
- 453 **Sano K**, Noshiro O, Katsuda K, Nishikori K, Maeno H. Dopamine receptors and dopamine-sensitive
454 adenylylase in canine caudate nucleus: Characterization and solubilization. *Biochemical*
455 *pharmacology*. 1979; 28(24):3617–3627.
- 456 **Schultz W**. Predictive reward signal of dopamine neurons. *Journal of neurophysiology*. 1998;
457 80(1):1–27.
- 458 **Schultz W**. Multiple dopamine functions at different time courses. *Annu Rev Neurosci*. 2007;
459 30:259–288.
- 460 **Schultz W**. Dopamine reward prediction-error signalling: a two-component response. *Nature*
461 *Reviews Neuroscience*. 2016; 17(3):183.
- 462 **Suaud-Chagny M**, Chergui K, Chouvet G, Gonon F. Relationship between dopamine release in the
463 rat nucleus accumbens and the discharge activity of dopaminergic neurons during local in vivo
464 application of amino acids in the ventral tegmental area. *Neuroscience*. 1992; 49(1):63–72.
- 465 **Sun F**, Zeng J, Jing M, Zhou J, Feng J, Owen SF, Luo Y, Li F, Wang H, Yamaguchi T, et al. A genetically
466 encoded fluorescent sensor enables rapid and specific detection of dopamine in flies, fish, and
467 mice. *Cell*. 2018; 174(2):481–496.

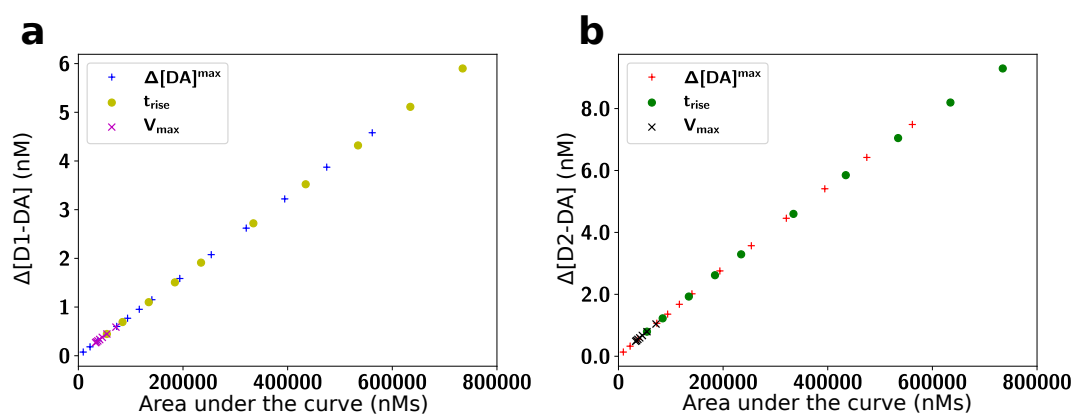
- 468 **Surmeier DJ**, Ding J, Day M, Wang Z, Shen W. D1 and D2 dopamine-receptor modulation of
469 striatal glutamatergic signaling in striatal medium spiny neurons. *Trends in neurosciences*. 2007;
470 30(5):228–235.
- 471 **Syed EC**, Grima LL, Magill PJ, Bogacz R, Brown P, Walton ME. Action initiation shapes mesolimbic
472 dopamine encoding of future rewards. *Nature neuroscience*. 2016; 19(1):34.
- 473 **Syková E**, Nicholson C. Diffusion in brain extracellular space. *Physiological reviews*. 2008; 88(4):1277–
474 1340.
- 475 **Tobler PN**, Fiorillo CD, Schultz W. Adaptive coding of reward value by dopamine neurons. *Science*.
476 2005; 307(5715):1642–1645.
- 477 **Venton BJ**, Zhang H, Garris PA, Phillips PE, Sulzer D, Wightman RM. Real-time decoding of dopamine
478 concentration changes in the caudate–putamen during tonic and phasic firing. *Journal of neuro-*
479 *chemistry*. 2003; 87(5):1284–1295.
- 480 **Yapo C**, Nair AG, Clement L, Castro LR, Hellgren Kotaleski J, Vincent P. Detection of phasic dopamine
481 by D1 and D2 striatal medium spiny neurons. *The Journal of physiology*. 2017; 595(24):7451–7475.



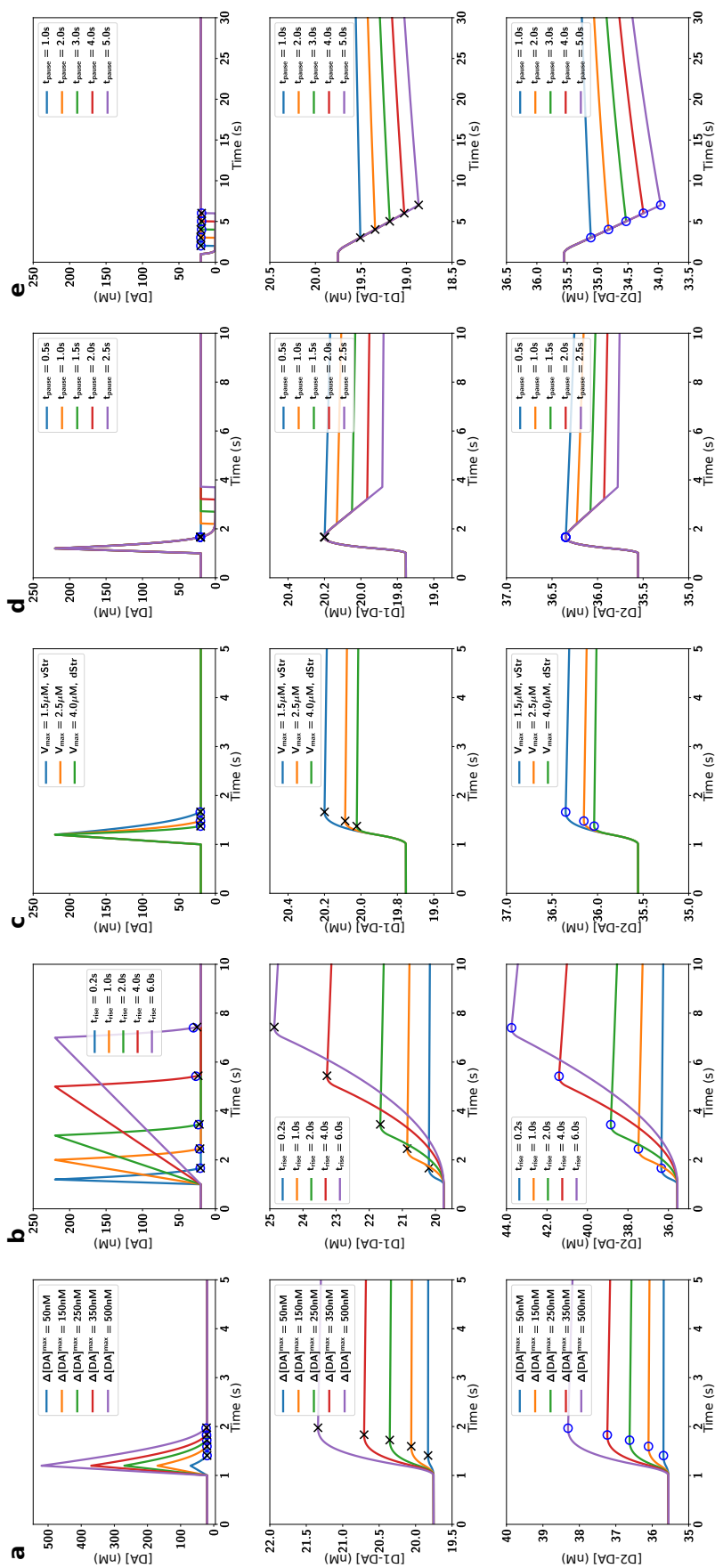
Supplemental Fig. 1. Similarities between D1 and D2 responses persist even if kinetics are much faster than our estimate. Fast kinetics were implemented by multiplying k_{on} and k_{off} by q as indicated, keeping K_D constant. Absolute D1R occupancy ([D1-DA]; left column) and D2R occupancy ([D2-DA]; right column) were examined for burst-pause DA signals (**a, b**), burst-only DA signals (**c, d**), and the behavioural sequence (**e, f**) (i.e. same simulation scenarios as in Fig. 1e and Supp. Fig. 5). D1Rs and D2Rs reacted very similarly to each other in all [DA] signal scenarios even if their kinetics were up to 100x faster because the difference between the aggregate D1 and D2 binding rates (Eq. 5) only differs by a factor of 1.5. Furthermore, the D2Rs do not show visible saturation effects even for $q = 100$. Faster kinetics mostly affected the amplitude of the receptor response and the time it takes to return to baseline receptor occupancy. However, only for $q = 100$ the pauses dropped slightly below baseline receptor occupancy (a, b). On a longer time scale with repetitive DA bursts (e, f) D1Rs and D2Rs integrated the DA bursts over time for $q = 1$ and $q = 2$. This is because the half-time of the receptors were 80 s (for $q = 1$), while the DA burst signal was repeated every 15 s. Thereby, [D1-DA] and [D2-DA] were dominated by the repetition of the signal rather than by the impact of individual DA burst signals. In contrast, for $q = 10$ the change in receptor occupancy was dominated by the single pulses, since the half-life time was 8s, whereby the receptors mostly unbind in between DA pulses.



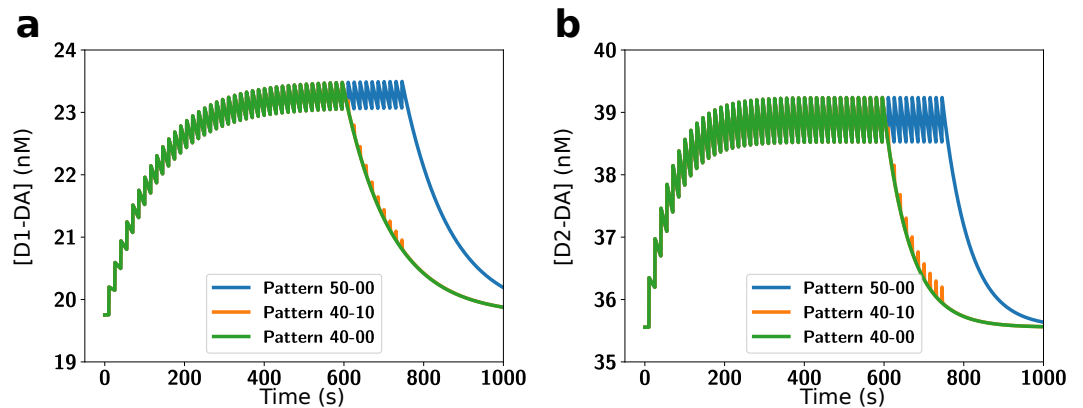
Supplemental Fig. 2. Burst-pulse DA signals did not lead to increased DA receptor occupancy after the signal, if the duration of the pause was matched to the amplitude of the burst. Panels indicate input DA signal (top) and resulting DA receptor-ligand binding (middle and bottom). The return to baseline after the pulse happened for both D1R and D2R since their aggregate kinetics are similar.



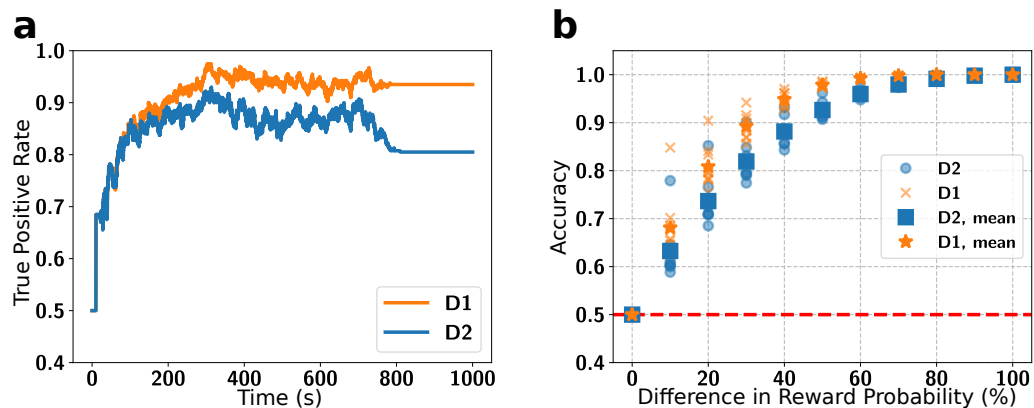
Supplemental Fig. 3. In the slow kinetics model the peak change in absolute receptor occupancy of D1Rs (a) and D2Rs (b) increased linearly with the area under the curve (AUC) of the DA pulses and parameter variations as in **Supp. Fig. 4a-c** (but with more parameter values). Here $\Delta[DA]^{max}$ marks burst-only DA pulses with varying peak amplitudes (50, 100, 150, 200, 250, 300, 350, 400, 500, 600, 700, 800, 900, 1000 nM), t_{rise} indicates ramping DA signals with with varying rise times (0.2, 0.5, 1.0, 1.5, 2.0, 3.0, 4.0, 5.0, 6.0, 7.0 s) and V_{max} indicates burst-only DA pulses with varying V_{max} (1.0, 1.5, 2.0, 2.5, 3.0, 2.5, 4.0 in $\mu M s^{-1}$). This indicates that D1Rs and D2Rs act as slow integrators of the DA signal and explains why ramps are an effective signal to occupy DA receptors.



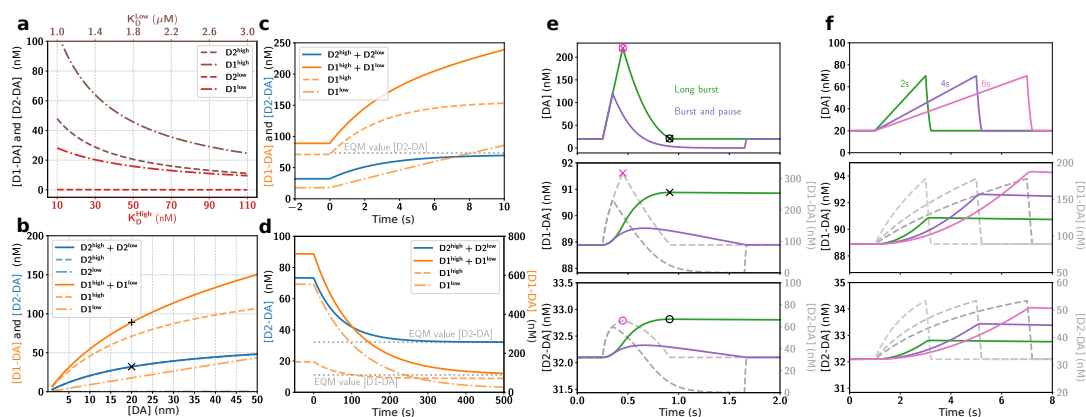
Supplemental Fig. 4. Parameter exploration for different DA signals (top row) with the resulting D1 (middle row) and D2 (bottom row) absolute receptor occupancy. The different input DA signals were burst-only with varying amplitude (**a**), ramp with varying rise time (**b**), burst-only with varying reuptake (**c**), burst-pause with varying pause duration (**d**), and pause-only with varying pause duration (**e**). Blue circles and black crosses mark the time points of maximum receptor occupancy for D1 and D2, respectively (**a-d**), and of minimal receptor activation in (**e**). Note that for both D1 and D2 the time of maximum receptor occupancy was near the end of the DA signal and that D1Rs and D2Rs behaved similarly independent of the specific parameters of the DA pulse.



Supplemental Fig. 5. Absolute receptor occupancy for D1Rs (**a**) and D2Rs (**b**) following a sequence of 50 events. The sequences consists of 50 rewarding long burst events (blue), 40 long burst and 10 burst-pause events (orange) and 40 long burst events followed by 10 none events (green). A sequence of events lead to an accumulation of occupied receptors, if the pause between long burst events were shorter than $\approx 2 \cdot t_{1/2}$. There was a plateau for the absolute amount of occupied receptor at the level at which the amount of receptors unbinding until the next burst is the same as the amount of receptors getting occupied during a long burst event. Burst-pause events did not lead to an accumulation of occupied receptors over time and were, except during the short bursts, identical to the none events (note the overlapping green and orange curves), in line with a "false alarm" signal over a range of occupancy levels.



Supplemental Fig. 6. (a) True positive rates for the classification in a sample session (70% vs 30% reward probability) based on the receptor occupancy (see Methods) of D1 (orange) and D2 (blue) receptors. After a short 'swing-in" the receptors could distinguish between a 70% and a 30% reward rate. **(b)** Accuracy of the classifier for a range of reward probability differences for the D1 (orange) and D2 (blue) receptors (see Methods) for individual sessions and corresponding session averages.



Supplemental Fig. 7. Impact of slow kinetics on D1R and D2R binding with 10% of D1R in a high affinity state ($D1^{high}$) and 10% of D2 receptors in a low affinity state ($D2^{low}$) (Richfield et al., 1989). The $D1^{high}$ state was modelled by increasing the on-rate of the D1R but keeping its off-rate constant, creating a receptor identical to the $D2^{high}$ receptor. We choose this model since the high affinity state kinetics of the D1R are currently unknown, and a faster on-rate could potentially have the strongest effect on our conclusions. Correspondingly, we modelled the $D2^{low}$ receptor as a D2R with slower on-rate, which was largely equivalent to simply reducing $[D2^{tot}]$ since the $D2^{low}$ receptors were predominantly unoccupied during baseline DA and bound only sluggishly to DA during phasic signals. The main effect of incorporating the different receptor affinity states was a change in the respective equilibrium values of absolute concentration of receptors bound to DA. **(a)** The receptor occupancy at baseline $[DA] = 20nM$ was dominated by the high affinity states for both receptors, even though only 10% of the D1R were in the high state. As in our default model also D1 receptors were occupied at baseline, enabling them to detect tonic DA signals. **(b)** The amount of bound D1R and D2R stayed within the same order of magnitude over a range of baseline [DA]. 'x' and '+' indicate the model default parameters. **(c)** As in the default model, for a large step up from $[DA] = 20nM$ to $[DA] = 1\mu M$, and **(d)** a step down from $[DA] = 1\mu M$ to $[DA] = 20nM$, D1 and D2 receptor occupancy approached their new equilibrium (EQM, grey dotted lines) only slowly (i.e. over seconds to minutes). As the $[D1-DA]$ changes were dominated by the $D1^{high}$ component, they were very similar to the D2R responses. **(e, f)** The effect of different phasic DA signals (top panels) was still very different in the slow kinetics model accounting for affinity states (coloured traces in middle and bottom panels; left scales) compared to the instant kinetics model (dashed grey traces, right scales). As in the default model, the timing of the maximum receptor occupancy ('x' and 'o' for D1 and D2, respectively) coincides for instant kinetics (purple symbols) with the [DA] peak (combined x and o in top panel), while for slow kinetics (black symbols) it coincides with the offset of the [DA] signal instead (combined x and o in top panel). The main difference to the default model is the higher occupancy of the D1R, caused by the $D1^{high}$ component. There is not a two-component unbinding since the $D1^{high}$ and $D1^{low}$ have similar off-rates, but differing on-rates. Overall, also for receptors with two affinity states, DA ramps are very effective in occupying the receptors.